Hindawi
Shock and Vibration
Volume 2017, Article ID 7982170, 12 pages
https://doi.org/10.1155/2017/7982170

Research Article

A Study on the Dynamic Behaviour of Lightweight Gears

Shadi Shweiki, Antonio Palermo, and Domenico Mundo

Department of Mechanical, Energy and Management Engineering, Università della Calabria, 87036 Rende, Italy

Correspondence should be addressed to Domenico Mundo; domenico.mundo@unical.it

Received 3 August 2017; Accepted 7 September 2017; Published 16 October 2017

Academic Editor: Matteo Filippi

This paper investigates the dynamic effects of mass reduction on a pair of spur gears. A one-Degree-of-Freedom (DOF) model of a mechanical oscillator with clearance-type nonlinearity and linear viscous damping is used to perform the investigations. One-dimensional (1D) gear pair models aim at studying the torsional gear vibrations around the rotational axes and can be used to simulate either gear whine or gear rattle phenomena. High computational efficiency is reached by using a spring-damper element with variable stiffness to model the gear meshing process. The angle-dependent mesh stiffness function is computed in a preparation phase through detailed Finite Element (FE) simulations and then stored in a lookup table, which is then interpolated during the dynamic simulation allowing for high computational efficiency. Nonlinear contact effects and influence of material discontinuities due to lightweighting are taken into account by FE simulations with high level of detail. Finally, the influence of gear body topology is investigated through a sensitivity analysis, in which analytical functions are defined to describe the time-varying mesh stiffness.

1. Introduction

Trends for emission limitations and fuel saving impose a more efficient energy exploitation in many sectors of mechanical engineering. Lightweighting is one of the strategies that can be adopted to reach this goal. Besides the environmental requirements, lightweighting is a key aspect in all the applications where the weight is a crucial aspect for the overall performance of the system, such as in aerospace and automotive industries. Geared power transmissions, which are key components in many mechanical systems, are not excluded from such a lightweighting trend.

Common lightweighting strategies are based on the reduction of gear thickness as well as on the manufacture of holes in the web of the gear. Although the use of lightweight gears in the transportation sector and in general machinery is continuously increasing, design problems related to the dynamic strength of such transmissions are not yet fully solved [1], requiring the development of simulation models able to predict the impact of different design choices (e.g., web thickness, number, position, and shape of the holes) on their vibration behaviour.

During gear meshing, complex phenomena occur simultaneously, such as nonlinear load-dependent contact deformations, friction, clearance, and time-varying mesh stiffness. Several simulation methods have been developed in the past years and, depending on the purpose of the investigation, each of them could represent the best trade-off between accuracy of predictive results and computational effort for a particular application.

Three-dimensional FE models for gear meshing analyses represent the most detailed simulation approach available nowadays [2]. The use of FEM for 3D static and dynamic contact/impact analysis of gear drives was proposed by Lin et al. in [3], while an example of FE-based optimization of gear microgeometry is reported in [4].

Analytical formulations and lumped-parameter modelling have been widely used to analyse gear dynamics thanks to their computational efficiency and capability to capture nonlinear phenomena in the dynamic behaviour [5]. Bonori et al. [6] used this formulation to optimize design parameters while Liu and Parker [7] proved its usefulness performing dynamic simulation of more complex systems. Recently, a dynamic simulation model based on a lumped-parameter formulation was developed by Zhang et al. to analyse the vibration modes of two-stage helical planetary gears used in cranes [8], while Dong et al. coupled lumped mass modelling and theoretical models for loaded and unloaded tooth contact analysis with the aim of investigating the vibration characteristics of power-split transmissions [9].

In comparison with FE approaches, lumped-parameter models have a high computational efficiency as key advantage, but an adequate description of the time-varying meshing stiffness and of the related dynamic excitation is required to enable accurate predictions of the system behaviour.

Analytical formulations of stiffness functions in helical gears were proposed by Cai in [10]. Recently, an insight on the role of time-varying mesh stiffness and on different calculation approaches was provided by Cooley et al. in [11]. In [12], a second-order polynomial function is used to describe the time-variant meshing stiffness that allowed introducing parametric excitation in the multibody model of a planetary gearbox, while a dedicated software for loaded tooth contact analysis in cylindrical gears is used in [13] for the same purpose.

Given the general nature of the method, detailed FE simulations enable mesh stiffness calculations and loaded tooth contact analysis without a priori assumptions, but at the cost of very high computational load. For this reason, hybrid approaches, combining FE and analytical modelling, have been developed [14, 15]. A gear dynamics simulation model, which uses a mortar-based mesh interface for hybrid FE/lumped-parameter models, was proposed and applied to analyse the dynamic behaviour of thin-rimmed geared systems in [16]. A combination of FE and lumped-parameter models was used by Ren et al. [17] to study the dynamic behaviour of a coupled gear-shaft-bearing-housing assembly by using the impedance synthesis method.

The Transmission Error (TE) is considered as one of the main excitation sources in a system where meshing gears are present [18]. It can be defined as the difference between the actual position of the driven gear and the position it would occupy if the gears were infinitely rigid and the teeth profiles perfectly conjugate. In solid, axisymmetric gears, the TE curve and the mesh stiffness function are typically dominated by the harmonic content at the meshing frequency. One of the effects of gear lightweighting is the occurrence of additional harmonic components at lower frequencies, originating from the nonuniform distribution of mass and stiffness along the gear blank.

In this paper, two different strategies for gear weight reductions are analysed. In the first case, gear lightweighting is obtained by reducing the web thickness resulting in a rimmed axisymmetric gear. A second lightweighting approach is based on material removal from the web through a series of holes or slots, which result in a rotational symmetry for the lightweight gear that influences the mesh stiffness and the TE of the gear pair. Such a phenomenon is investigated through nonlinear FE simulations that allow computing the Static Transmission Error (STE) curves of the different gear pairs, from which the angle-dependent mesh stiffness is derived. Subsequently, the statically computed curves are used in a 1D lumped-parameter model to simulate the dynamics of the different lightweight gear pairs. Thanks to the described approach, detailed and time-consuming simulations are limited in a preprocessing phase without affecting the computational efficiency of the analytical model, while the dynamic effects of the different gear topologies are well captured by the latter model.

Table 1: Main properties of the gears.

Parameter	Value
Teeth number	57
Normal module	2.6 mm
Normal pressure angle	20 deg
Tip diameter	154.5 mm
Root diameter	141.7 mm
Face width	23 mm
Contact ratio	1.45
Working centre distance	150 mm
Material	Steel

2. STE Estimation in Lightweight Gears by Nonlinear FE Simulations

An analysis of how the different strategies for lightweight design influence the static response of a gear pair is done by estimating the STE curves through nonlinear FE simulations, for which high-detail models of the meshing gears have been built.

Four case studies, consisting of different gear pairs, are analysed. In each pair, a solid blank gear is meshing with a lightweight gear, with a different layout. The four gear pairs analysed through nonlinear FE simulations are shown in Figure 1. In the gear pairs of Figures 1(a) and 1(c), the blank of the lightweight gear is axisymmetric; that is, mass reduction is achieved by reducing the depth of the rim, while in the other two case studies gear lightweighting is achieved through eight circular holes and three slots in the blank, as shown in Figures 1(b) and 1(d), respectively. The last gear pair represents a case of extreme lightweight design, which will be analysed along with the others to highlight the effects of increased blank flexibility on the mesh stiffness and, subsequently, on the dynamic response of the system. The two lightweight gears with axisymmetric geometry, shown in Figures 1(a) and 1(c), have been designed as to have the same overall mass of the lightweight gears with 8 holes and 3 slots, respectively. Gear (a) can be directly compared to gear (b), except for the absence/presence of the holes and their effect on blank stiffness; the same holds for gears (c) and (d).

The FE models of the four meshing gear pairs, shown in Figure 1, were created by using 8-node hexahedral elements, while the main design specifications are reported in Table 1.

In the FE model of the gear pairs, supporting shafts were represented as infinitely rigid by rigidly constraining all the DOFs of the gear bore nodes to a master node located in the centre of the gear and constrained with rigid body elements. A loading torque equal to 350 Nm was applied to the master node located at the pinion centre, for which the rotational DOF is left unconstrained. With the aim of generating STE curves, different nonlinear FE static simulations were performed for each gear pair, by positioning the two gears in a discrete number of equally spaced angular positions in the

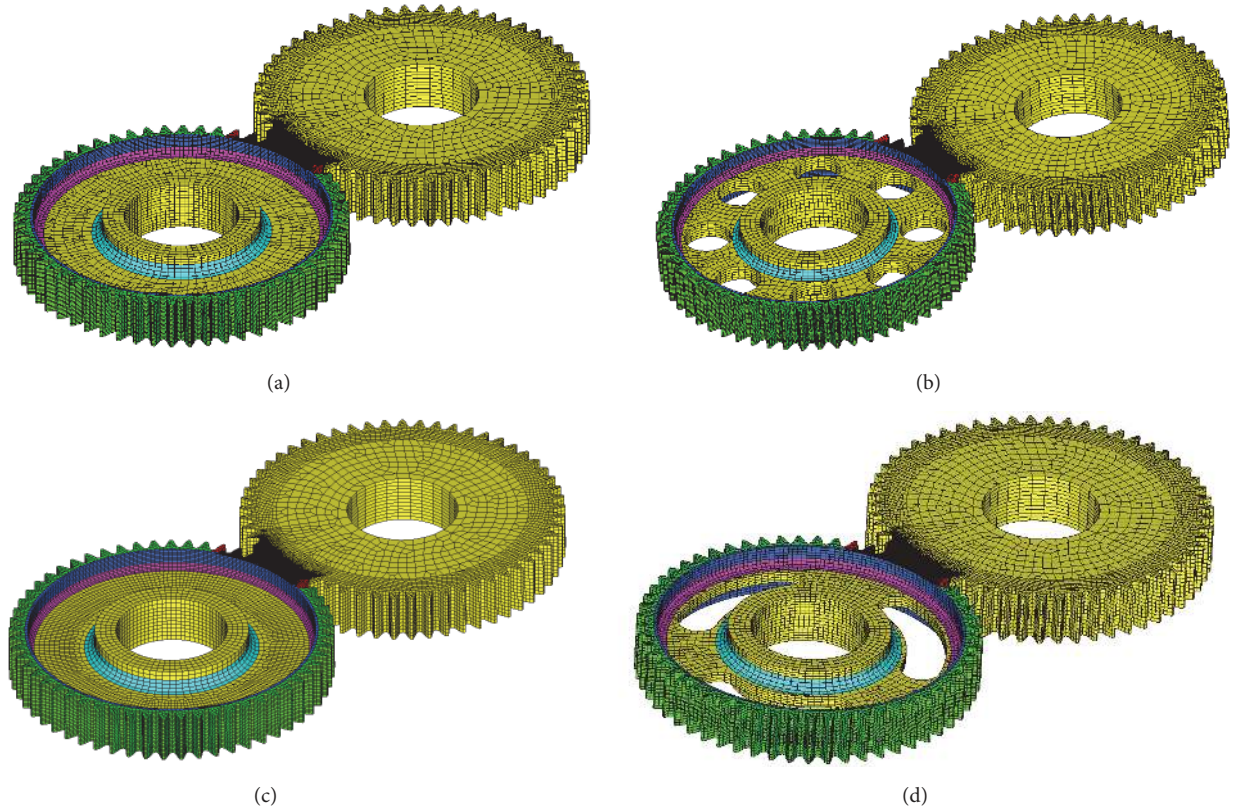

Figure 1: FE models of the four gear pairs analysed: (a) and (c) have an axisymmetric design for the lightweight gear, while 8 holes and 3 slots enable mass reduction in (b) and (d), respectively, with different degrees of discrete rotational symmetry. Gears (a) and (b) are designed to have the same total mass; the absence/presence of the holes cause different effect on blank stiffness; the same holds for gears (c) and (d).

angular period of the gear pair. In each angular configuration, one point of the STE curve is computed according to the following equation:

$$\mathrm{TE} = r_{bG}\theta_G - r_{bP}\theta_P, \tag{1}$$

where θ_P and θ_G represent the rotation of the pinion and of the gear, respectively, while r_{bP} and r_{bG} are their base radii. In the specific cases analysed in this paper, θ_P is the final rotational displacement of the pinion master node after load application, while θ_G is equal to zero, considering the constraining condition of the gear, in which the master central node is held stationary during the simulations. Having identical tooth geometry, the two gears have the same base radius.

In order to reduce the computational time, the FE model of each gear was divided into regions of different mesh size. In the regions close to the tooth contact area, where a detailed description of the geometry is required to properly capture contact phenomena, the element size was set to 0.11 mm, based on a convergence analysis [4]. Considerably coarser mesh was created in the regions that are sufficiently far from the meshing teeth. Since the computational complexity is strictly dependent on the number of nodes in the model, several models were created for each nonaxisymmetric gear, as to limit the number of teeth with fine mesh to 5, that allow for simulating 3 meshing cycles. A total of 7 and 19 models were created for the gear with 8 holes and with 3 slots, respectively. An example of the results obtained from the nonlinear FE simulations in a region of an axisymmetric gear close to the meshing area is shown in Figure 2, while Figure 3 highlights the effects of material removal from the blank on the local and on the global deformation of the lightweight gear with holes. It appears, in fact, that lack of material in the region close to the meshing teeth causes higher deflections compared to the situation in which the meshing teeth are close to a region of the web in which no holes are present.

By postprocessing the results of the static simulations, the STE curves for each pair of meshing gears were derived. From the STE curves shown in Figure 4, it is possible to appreciate that the effects of blank topology of the lightweight gear on the mesh stiffness of the gear pairs are significantly different in the four case studies.

Figures 4(a) and 4(c) show the STE curves estimated for the gear pairs of Figures 1(a) and 1(c), respectively. The two curves are periodic with the mesh frequency and do not exhibit lower frequency harmonic components. The effects of the holes and of the slots are clearly visible in the curves of Figures 4(b) and 4(d), where the additional low-frequency components significantly change the shape of the curves.

Such observations are confirmed by the results of the FFT analysis shown in Figure 5, where the frequency content of the STE curves for the nonaxisymmetric gears shows the presence of low-frequency components, with an angular

Table 2: Main properties of the gears that will be used in the analytical model for dynamic simulations.

Parameter	Gear (a)	Gear (b)	Gear (c)	Gear (d)
Gear inertia	0.0041 kg × m^2	0.0041 kg × m^2	0.0038 kg × m^2	0.0038 kg × m^2
Average mesh stiffness	2,72E + 08 N/m	2,18E + 08 N/m	2.42E + 08 N/m	1,35E + 08 N/m
Average resonant frequency	3258 Hz	2962 Hz	3030 Hz	2345 Hz
STE amplitude at meshing frequency	3.776 μm	3.663 μm	3.921 μm	3.894 μm
STE amplitude at blank angular frequency	0 μm	1.794 μm	0 μm	9.584 μm

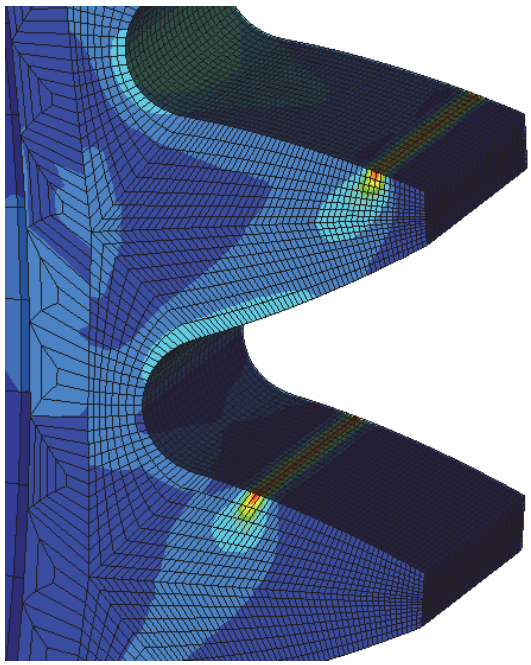

Figure 2: Example of stress distribution estimated by nonlinear FE simulation for the lightweight gear shown in Figure 1(b) in a given configuration.

frequency equal to the number of material discontinuities in the blank (holes or slots) and its multiples.

From the static results shown above, the mesh stiffness that will be used as input for the dynamic simulations is derived. For the purpose of calibrating the analytical model, the gears are lumped into rigid bodies with inertia and stiffness proprieties derived from the FE models and reported in Table 2.

3. Lumped-Parameter Modelling and Dynamic Analysis of a Lightweight Gear Pair

The model described by the following equations is derived from the one proposed in [5] and is intended to describe the relative motion between two gears in dynamic conditions. The joints are supposed to be perfectly rigid, so that no motion of the gears is allowed except for the rotation along their rotational axis. Gear meshing is modelled by a single spring-damper system acting along the line of action of the gear pair. The use of one single spring representing both the blank stiffness and the teeth contact stiffness can be justified by the consideration that the meshing frequency and its harmonics are almost identical for all the gear pairs analysed in the paper, indicating that in static condition the contribution to the TE of the tooth stiffness is not significantly affected by the holes or the slot in the gear body. Additional dynamic contributions coming from the tooth mode shapes are neglected in this work, the focus being on the impact of blank topology on the dynamic behaviour of the gear pair, which can be captured by the torsional model used in this work.

In this way, the relative motion between the gears is described as a linear displacement along the line of action. Consistently, the applied torque and the rotational inertia are converted, respectively, in a linear force acting along the line of action and in an equivalent mass. The transformation from a rotational inertia to an equivalent mass is done considering the gears as homogeneous discs, and extracting their inertia properties from a CAD model, while the equivalent mass of the 1 DOF system, which is represented in Figure 6, is calculated starting from the mass values estimated for each gear.

The dynamic behaviour of this 1-DOF system, which considers a pair of identical gears, is governed by the following equation of motion:

$$m\ddot{x} + 2\zeta\dot{x} + k\left[\mathrm{PC}\left(t\right)\right] g\left[x\left(t\right)\right] = F\left(t\right), \tag{2}$$

where x is the linear relative displacement of the equivalent gear pair along the line of action and represents the Dynamic Transmission Error (DTE) in the system; $\dot{x}$ and $\ddot{x}$ are its first and second time derivatives; m is the equivalent mass of the system; and ζ is a damping coefficient introduced in the model to consider losses during tooth meshing. The model parameter $k[\mathrm{PC}(t)]$ is intended to represent the time-varying mesh stiffness derived from the STE curves calculated as described in Section 2. The mesh stiffness is a function of the instantaneous position of the contact point PC(t) along the mesh cycle, which is derived as

$$\mathrm{PC}\left(t\right) = \frac{1}{\theta_{P1}}\left[\theta_1\left(t\right) - \mathrm{floor}\left(\frac{\theta_{1(t)}}{\theta_{P1}}\right)\theta_{P1}\right], \tag{3}$$

where $\theta_1(t)$ is the actual value of the rotational angle and θ_{P1} is the angular period of the STE curve. The obtained value of PC is between 0 and 1. When an axisymmetric gear is analysed, the angular period corresponds with the length of the meshing cycle, because no harmonic components due to the gear body discontinuities are present in the STE curve of the gear pair. In this case, the variability of the mesh stiffness

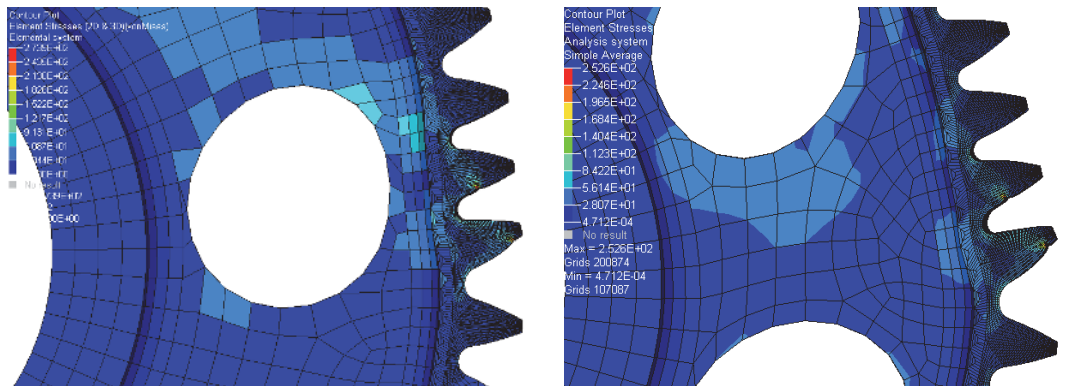

(a) (b)

Figure 3: Example of stress distribution and static deformation of the gear with 8 holes in two angular configurations of the gear pair: loaded teeth are close (a) and far away (b) from a hole in the blank.

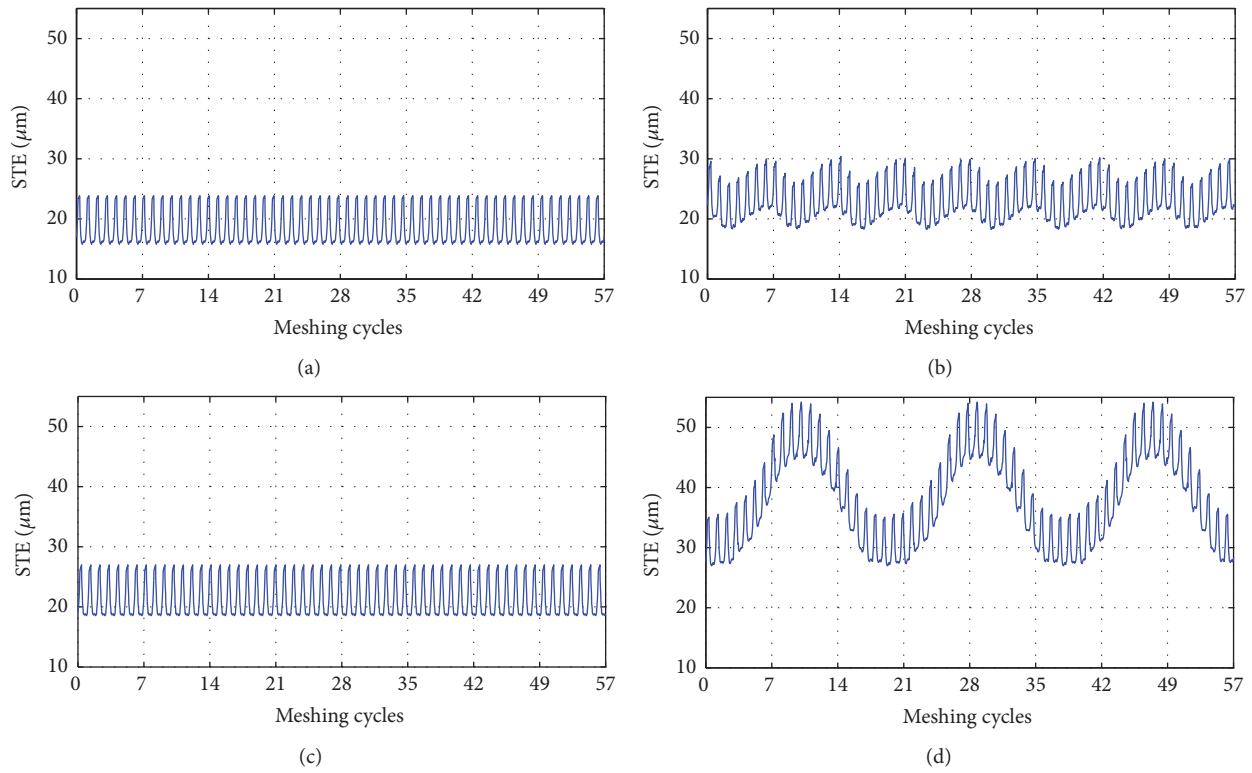

Figure 4: STE curves of the analysed gear pairs computed through nonlinear FE simulations for the gear pairs (a), (b), (c), and (d) in Figure 1.

is given mainly by the variable number of tooth pairs in contact, which results in a dominant harmonic component in the STE at the meshing frequency and additional harmonic components. When gears with material discontinuities in the blank, that is, holes or slots, are analysed, the angular period has to be extended in order to capture the entire frequency content of the STE curve. An entire revolution of the gear has to be analysed in the case in which the teeth number is not an integer multiple of the hole number, while symmetry exploitation can be sought in those cases where the tooth number is a multiple of the hole number, as for the case of the gear with 3 slots.

The periodic mesh stiffness k is derived as a function of the rotational angle from the STE curves through the following equation:

$$k\,(\mathrm{PC}) = \frac{F_{\mathrm{tt}}}{\mathrm{STE}\,(\mathrm{PC})}, \tag{4}$$

where F_{tt} is the magnitude of the tangential contact force used for estimating the STE curves. The hypothesis behind this approach is that the dependencies of the obtained STE values with the transmitted load are negligible in a small load interval around the nominal condition. No microgeometry

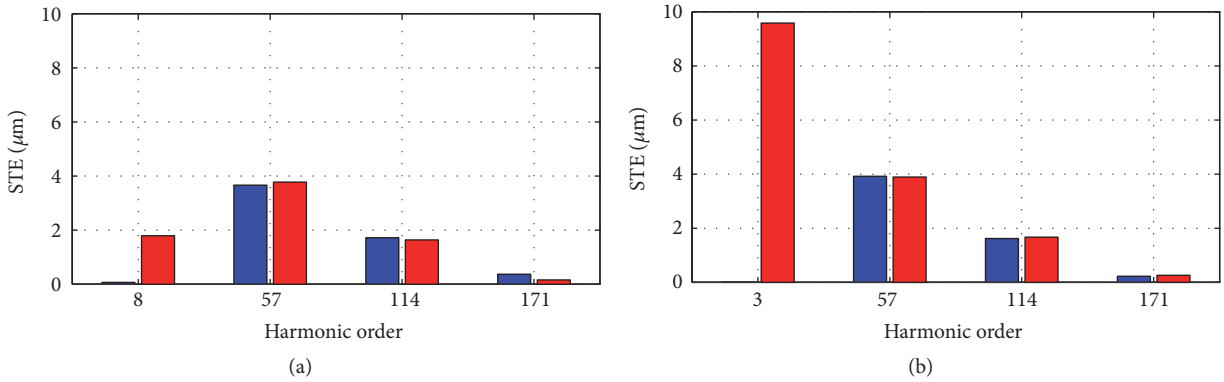

Figure 5: Amplitude of different harmonic components obtained from FFT of the STE curves computed for gear pairs (a and b) (a) and for gear pairs (c and d) (b). The rotational speed is kept constant in each simulation. Blue histograms refer to the axisymmetric gears.

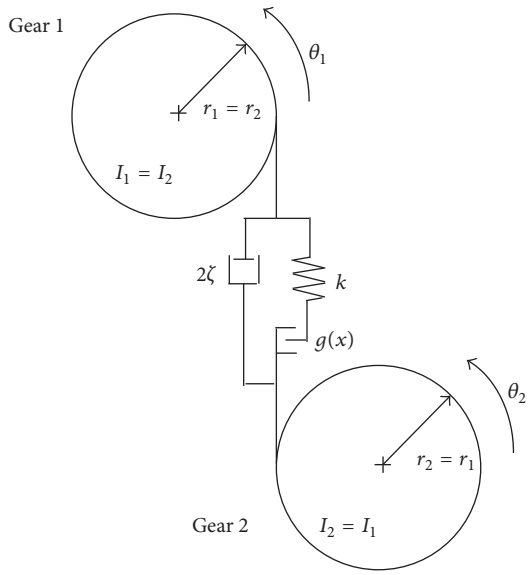

Figure 6: Dynamic representation of the 1D model of meshing cylindrical gears.

modifications are applied on the teeth and the nonlinear dependencies of the STE with the applied load are not taken into account. The applied torque corresponds to the one used in the STE calculation phase. In line with the assumption of perfect joints, no further dependencies of the STE on the relative misalignment between the gears are considered.

The mesh stiffness values are stored as function of the relative angular position of the gears in lookup tables, which are then interpolated during the dynamic simulation.

The formulation of (2) allows also modelling the backlash b between the gears introducing the restoring function $g[x(t)]$, which is the following function of the equivalent relative displacement between the gears [5]:

$$g\left[x\left(t\right)\right] = \begin{cases} x\left(t\right) - b, & x\left(t\right) > b, \\ 0, & \left|x\left(t\right)\right| \leq b, \\ x\left(t\right) + b, & x\left(t\right) < -b. \end{cases} \quad (5)$$

The restoring function allows considering contact losses between the teeth, by bringing the value of the mesh stiffness to zero when the relative displacement is below the backlash threshold. This condition means that there is no contact between the teeth and consequently no elastic meshing force acting on the bodies. When the instantaneous relative displacement assumes a value higher than the imposed backlash, the restoring function allows considering only the effective penetration between the teeth in contact, subtracting the backlash from the estimated relative displacement.

The external force $F(t)$ in (2) represents the loading force in the system. In general, a time-varying load can be considered in the model, but in the work presented in this paper it is considered to be constant, based on the assumption that the imposed value of transmitted torque by the gears is constant.

The instantaneous acceleration value $\ddot{x}$ is computed numerically by using a fixed step explicit Runge-Kutta algorithm. Dynamic simulations are performed considering a constant applied torque of 350 Nm and a linearly increasing speed from 0 to 5000 rpm in 200 seconds. The fixed time-step is set to 2 microseconds and corresponds also to the sampling period. This grants a maximum observable frequency of 250 kHz, which is sufficiently high to reconstruct impulsive phenomena and to capture the significant harmonics of the gear mesh frequency.

The actual value of the rotational speed given as revolutions per minute is converted into a meshing frequency value by considering the teeth number. The position along the mesh cycle is obtained by integrating the instantaneous meshing frequency value.

The obtained time histories of the DTE are then analysed in terms of root mean square (RMS) of the oscillating component in each mesh cycle versus the meshing frequency.

One model is created for each of the four gear pairs, with inertia and stiffness (STE) properties derived as described in Section 2.

The RMS of the steady-state oscillating component of the estimated DTE is reported in Figure 7. The results of Figures 7(a) and 7(c), corresponding to the two axisymmetric gears, and of Figure 7(b), corresponding to the gear with 8 holes, show a clearly visible jump in correspondence with the

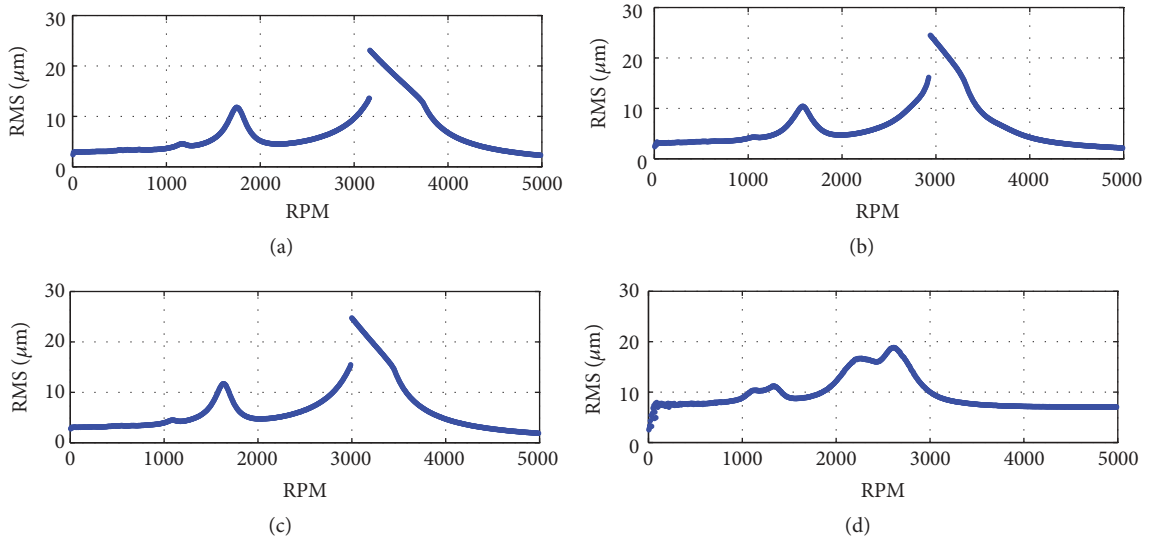

Figure 7: RMS of DTE obtained by using the different STE curves computed for the four gear pairs shown in Figure 1.

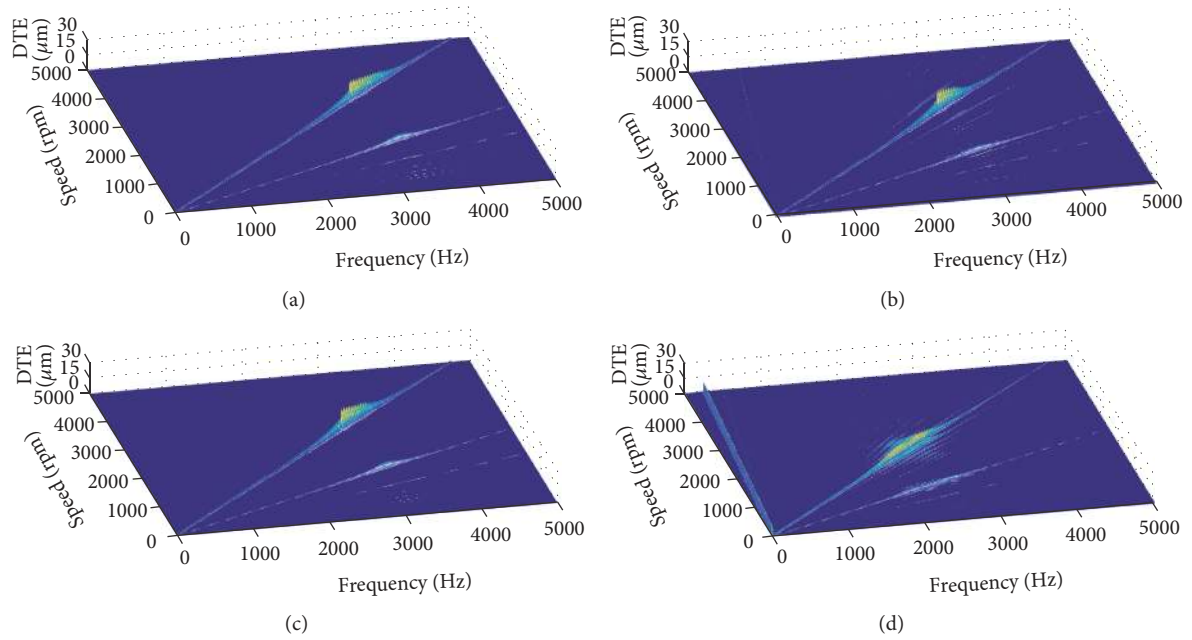

Figure 8: Waterfall diagram of the DTE for the four gear pairs analysed.

resonance frequency. The jump phenomena, which are due to loss of contact and are a typical clearance-type nonlinearity, disappear in the dynamic response of extremely flexible gear pair (d), in which the lightweight design is achieved through three slots.

By comparing the DTE estimated for gear pairs (a-b) and (c-d), which have identical inertia properties, different amplitude in the RMS of the dynamic response is observed in the analysed frequency range. It is worth to notice also that the nonaxisymmetric design has a lower average mesh stiffness as compared to the axisymmetric gear with the same mass reduction. For a given mass reduction, the lower value of the average mesh stiffness determines a frequency shifting towards lower values and a modification of the amplitude of jump phenomena in the dynamic response. Loss of contact phenomena appear less significant in gear pairs with nonaxisymmetric lightweight gear and disappear for the gear pair (d).

A thorough comparison can be done considering the waterfall diagrams shown in Figure 8. When the gear lightweighting is achieved by discontinuities in the gear blanks, the low-frequency harmonic components of the STE shown

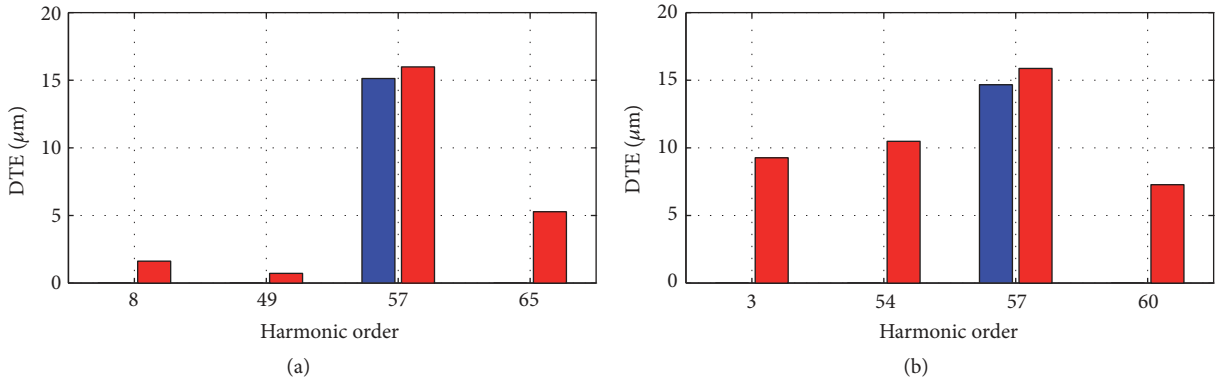

Figure 9: Amplitude of different harmonic orders obtained from FFT of DTE curves obtained for gear pair (a and b) (a) and for gear pair (c and d) (b). The rotational speed is kept in each simulation constant. Blue histograms refer to axisymmetric gears.

in Figure 5 cause additional excitation orders, while sideband effects show up in the regions where the meshing order excites the resonance of the system.

To further analyse the effects of lightweight design on the dynamic behaviour of each gear pair, constant-velocity simulations, at a speed where the meshing frequency is slightly below the gear pair resonance frequency, have been executed. The results are summarized in Figure 9(a) for gear pairs (a) and (b) and in Figure 9(b) for gear pairs (c) and (d), which show the results of the FFT analysis of the DTE curves estimated for the four gear pairs in steady-state conditions. Only the amplitude of the meshing order and its sidebands, along with the orders due to the holes, are reported.

Gear pairs (b) and (d) (red) exhibit a different dynamic behaviour as compared to the gear pairs with an axisymmetric design (blue). Due to the additional excitation orders shown in the waterfall diagrams, significant harmonic components due to the holes and slots are observed at low frequencies. Specifically, for the extreme lightweight design of gear pair (d) in Figure 9(b), the system response excited by the order of the slots is comparable with the one of the meshing order, even if the latter excites the resonance of the system. Clear sidebands around the meshing frequency and its harmonics can be appreciated as well.

4. Parametric Study

The simulation results shown in the previous sections demonstrated that the presence of holes in the gear blank influences the average value of the mesh stiffness and the shape of the STE curve, in which an important harmonic component shows up at the angular frequency of the gear blank geometry (linked to the number of holes), on top of the harmonic component at the meshing frequency (linked to the number of teeth). With the aim of investigating the impact of such modifications of the STE curves on the dynamic response of the gear pair, a parametric model of the STE curve is defined as

$$\begin{aligned} \mathrm{STE}(\mathrm{PC}) = {} & \mathrm{STEav} + \mathrm{STEh} * \cos(N\mathrm{h} * \mathrm{PC}) + \mathrm{STEm} \\ & * \cos(N\mathrm{t} * \mathrm{PC}), \end{aligned} \tag{6}$$

Table 3: Ranges in which the STE parameters are varied.

	STEav	STEh	STEm
Min (m)	18	0	2
Max (m)	38	10	6

where STEav is the mean STE value, while STEh and STEm are the harmonic components at the hole angular order and at the meshing order, respectively. Nh = 8 and Nt = 57 are the number of holes and the number of teeth, respectively, while the ranges that have been set for the three STE parameters are shown in Table 3.

The STE curves, analytically generated through (6) and by varying the parameters in the ranges of Table 3, are represented in Figure 10. The harmonic component in the STE curve with the angular frequency corresponding to the number of discontinuities in the gear web is intended to represent the harmonic fluctuation in the STE curve due to the presence of the discontinuities. Its amplitude is changed from curve to curve in order to replicate the effect of positioning and sizing of holes in real design.

The harmonic component of the STE curve at the tooth meshing frequency is mainly due to the change in the instantaneous number of meshing teeth between 1 and 2 in the case studies illustrated in this paper.

From each of the analytically generated STE curves, one mesh stiffness function is derived and used in the gear pair model of (2). In all the simulations, the damping coefficient is varied in such a way that a modal damping ratio of around 6% for the equivalent Linear Time-Invariant (LTI) system is obtained. The inertia values are kept constant during the analysis, being the focus of the simulation campaign on the relative importance of the harmonic content of the internal excitation.

4.1. Effect of the Average STE Value. The results shown in Figure 11 represent the different dynamic responses of the system for different values of the average STE value.

Each point of the curves represents the RMS value of the steady-state forced response in terms of DTE oscillating

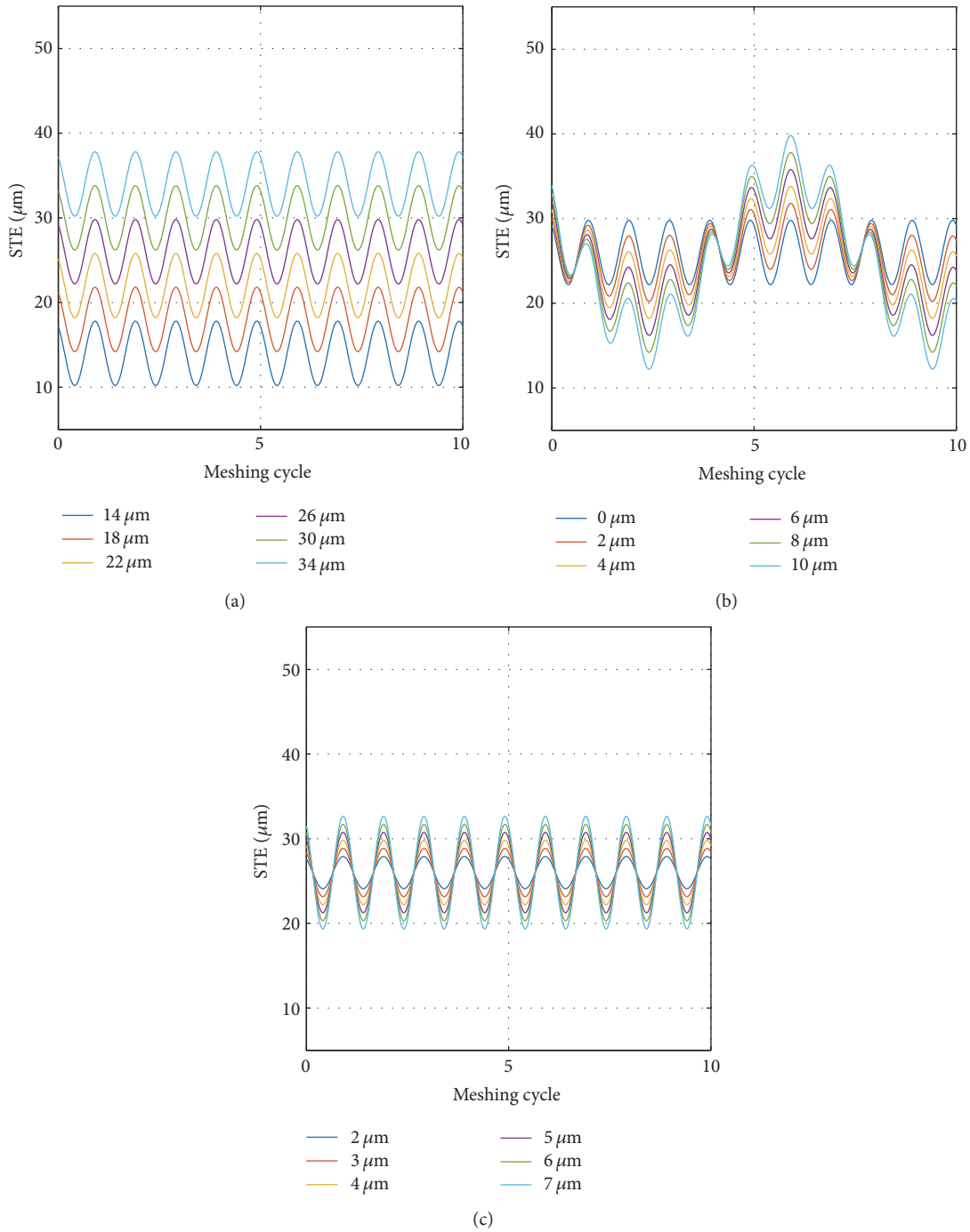

FIGURE 10: Portions of STE curves analytically generated by (a) varying the average value of the STE, (b) varying the amplitude of the harmonic component at the angular frequency of the holes, and (c) varying the amplitude of the harmonic component at the angular frequency of the meshing teeth.

component in a mesh cycle. It is worth to say that higher values in the STE correspond to lower values of mesh stiffness. The tooth-passing component and the order of the holes are kept fixed to a reference value of 4 μm and 0 μm, respectively. In particular, the latter value corresponds to a configuration in which no holes are present in the gear blank.

The effects of an increasing average value of the STE, shown in Figure 11, can be summarized in a shift of the resonant frequency of the system to lower values, an increase in the peak value of the DTE, and a reduction of the frequency range in which teeth lose contact.

4.2. Effect of STE Harmonic Component at the Mesh Frequency. The effects of the amplitude of the meshing harmonic component of the STE are shown in Figure 12. As above, the simulation parameters are unchanged for all the simulations

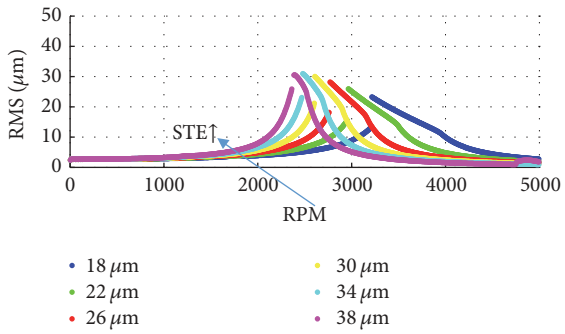

Figure 11: RMS of the different DTE curves obtained by using different average values of STE.

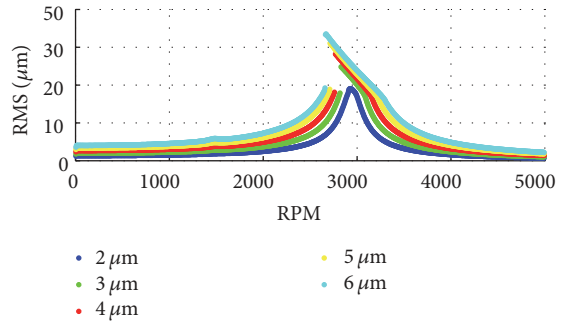

Figure 12: RMS of the different DTE curves obtained by using different values of the amplitude of the harmonic component at the meshing frequency.

of the campaign except for the amplitude of the harmonic component at the angular period corresponding to the tooth meshing period.

Increasing the amplitude for the meshing harmonic component of the STE does not alter the resonance frequency of the equivalent LTI system; therefore all curves remain centred around the same resonance frequency. Furthermore, higher meshing harmonic amplitudes correspond to a proportional increase in the dynamic response in the linear dynamic region. It is worthy to notice that such increase in the dynamic response makes the gears lose contact at a lower frequency. Similarly, gears regain full contact later at higher frequencies.

4.3. Effect of STE Harmonic Component due to Discontinuities in the Gear Web. The effects of varying the amplitude of the harmonic component of the STE due to discontinuities in the gear web are shown in Figure 13.

It is important to highlight that the average value of the STE curve is not affected by the amplitude of the contribution coming from the material discontinuities in the lightweight gear blank. Consistently, the jump phenomenon is not modified in its amplitude by the presence of the holes. From Figure 13 it is clearly visible that additional amplifications in the RMS curve are directly dependent on the amplitude of this additional harmonic component. These amplifications have the characteristic of modulation sidebands of the DTE

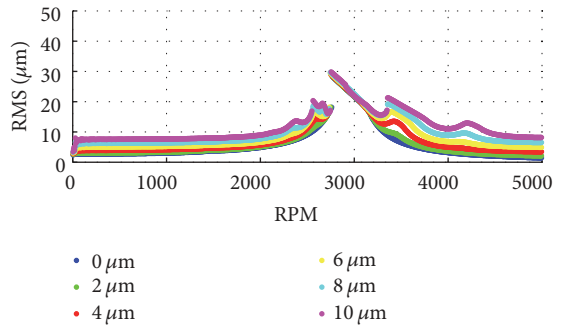

Figure 13: RMS of the different DTE curves obtained by using different values of the amplitude of the component due to discontinuities in the gear web.

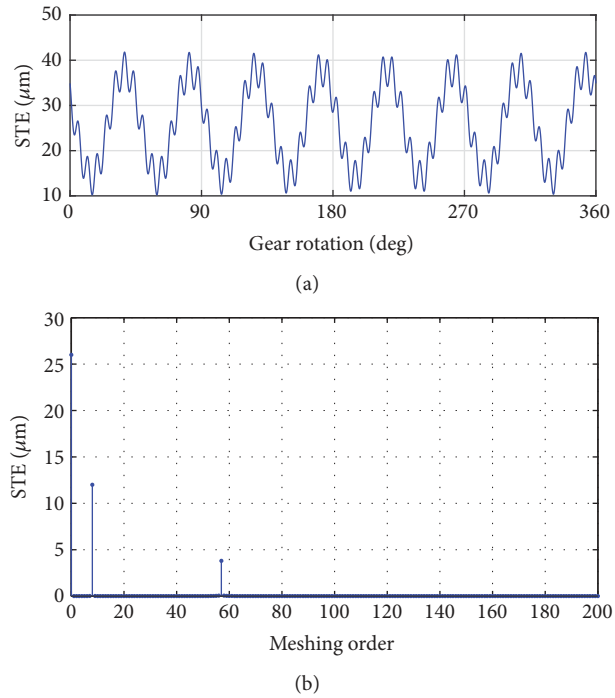

Figure 14: Example of STE curve obtained for STEh = 10 μm and STEm = 3.8 μm. STE curve (a) and the results of an FFT analysis in the angle domain (b).

curve. Additional jump phenomena appear when a sideband due to the web discontinuities matches the resonance frequency of the gear pair.

Considering Figure 14, where an example of STE curve used in the analysis is reported together with its FFT analysis in angle domain, it is possible to notice that no amplitude modulation sidebands are present since the harmonic components shown in Figure 14(b) are corresponding, by analytical definition, to the meshing and to the hole components only. Sidebands are instead clearly visible in the FFT analysis of the mesh stiffness derived from the STE curve according to (4) and shown in Figure 15. Dynamic sideband amplifications are observed also in the waterfall diagram shown in Figure 16.

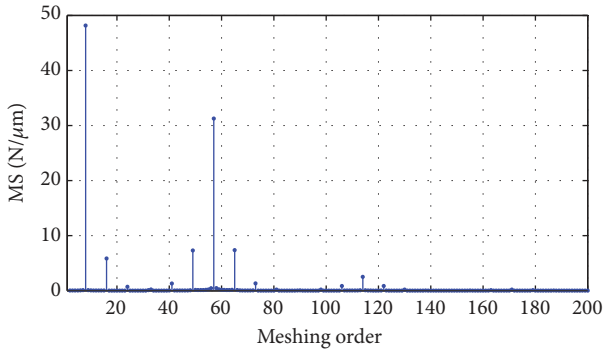

Figure 15: FFT analysis of the mesh stiffness obtained from STE curves of Figure 14.

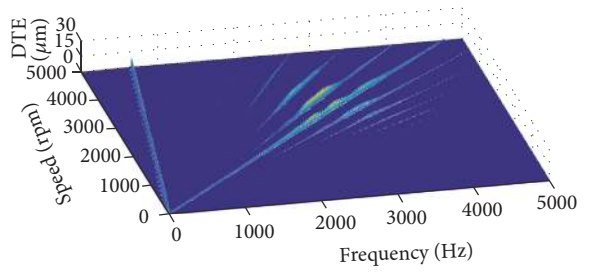

Figure 16: Waterfall diagram of the DTE of the system obtained using STE curves reported in Figure 14.

5. Conclusions

In this paper the effects of blank lightweighting on the static and on the dynamic behaviour of a pair of meshing gears have been investigated by combining nonlinear FE simulations and lumped-parameter modelling.

In the first part of the paper four case studies have been analysed, with different lightweight designs: in two cases, an axisymmetric lightweight gear, with reduced blank thickness, engages with a solid gear; in the other cases, weight reduction is achieved in the lightweight gear through holes and slots in the blank achieving the same mass reduction as in the corresponding axisymmetric gear. The STE curves are derived through a series of nonlinear FE simulations, allowing for a detailed description of the impact of gear blank topology on the mesh stiffness. The latter is then used in a lumped-parameter formulation for nonlinear dynamic analysis.

The simulation results, analysed in both time and frequency domain, show that the dynamic behaviour of the gear pairs with material discontinuities in the web is significantly different from the one of the axisymmetric gear pair. The variability of the average mesh stiffness during gear rotation, in fact, causes additional excitation orders and produces modulation effects in the dynamic response of the transmission analysed in terms of DTE. The frequency and amplitude of these contributions are dependent on the topology of the gear blank and on the harmonic content of the STE, which is well captured by the nonlinear FE simulations. Sideband effects show up in the regions where the meshing order excites the resonance of the system. One of the most interesting phenomena linked to gear dynamics, that is, jumps in the RMS of the DTE due to tooth loss of contact, is significantly affected by blank topology and seems to completely disappear in extremely lightweight design.

To provide an insight of the observed phenomena, dynamic simulations with analytically generated STE functions have been performed in order to analyse the effects of the additional STE harmonic component, due to the discontinuities in the gear blanks. The results showed additional amplifications in the RMS curves, due to the modulation effects of the holes on the mesh stiffness of the gear blank and the consequent sideband phenomena.

Conflicts of Interest

The authors declare that they have no conflicts of interest.

Acknowledgments

The research leading to these results has received funding from the People Programme (Marie Curie Actions) of the European Union's Seventh Framework Programme FP7, 2007–2013, under REA Grant Agreement no. 324336, DEMETRA: Design of Mechanical Transmissions: Efficiency, Noise and Durability Optimization.

References

[1] S. Li, "Experimental investigation and FEM analysis of resonance frequency behavior of three-dimensional, thin-walled spur gears with a power-circulating test rig," *Mechanism and Machine Theory*, vol. 43, no. 8, pp. 934–963, 2008.

[2] F. L. Litvin and A. Fuentes, *Gear Geometry and Applied Theory*, Cambridge University Press, Cambridge, UK, 2004.

[3] T. J. Lin, H. Ou, and R. F. Li, "A finite element method for 3D static and dynamic contact/impact analysis of gear drives," *Computer Methods Applied Mechanics and Engineering*, vol. 196, no. 9–12, pp. 1716–1728, 2007.

[4] J. A. Korta and D. Mundo, "Multi-objective micro-geometry optimization of gear tooth supported by response surface methodology," *Mechanism and Machine Theory*, vol. 109, pp. 278–296, 2017.

[5] G. W. Blankenship and A. Kahraman, "Steady state forced response of a mechanical oscillator with combined parametric excitation and clearance type non-linearity," *Journal of Sound and Vibration*, vol. 185, no. 5, pp. 743–765, 1995.

[6] G. Bonori, M. Barbieri, and F. Pellicano, "Optimum profile modifications of spur gears by means of genetic algorithms," *Journal of Sound and Vibration*, vol. 313, no. 3–5, pp. 603–616, 2008.

[7] G. Liu and R. G. Parker, "Nonlinear dynamics of idler gear systems," *Nonlinear Dynamics*, vol. 53, no. 4, pp. 345–367, 2008.

[8] L. Zhang, Y. Wang, K. Wu, and R. Sheng, "Three-Dimensional Modeling and Structured Vibration Modes of Two-Stage Helical Planetary Gears Used in Cranes," *Shock and Vibration*, vol. 2017, Article ID 9864959, 2017.

[9] H. Dong, Y. Cao, and Z. Fang, "Dynamic Vibration Characteristic Analysis for the Power-Split Transmission System Based on Loaded Tooth Contact Analysis," *Shock and Vibration*, vol. 2015, Article ID 871894, 2015.

[10] Y. Cai, "Simulation on the rotational vibration of helical gears in consideration of the tooth separation phenomenon (a new stiffness function of helical involute tooth pair)," *Journal of Mechanical Design*, vol. 117, no. 3, pp. 460–469, 1995.

[11] C. G. Cooley, C. Liu, X. Dai, and R. G. Parker, "Gear tooth mesh stiffness: A comparison of calculation approaches," *Mechanism and Machine Theory*, vol. 105, pp. 540–553, 2016.

[12] W. Yang and D. Jiang, "An improved rigid multibody model for the dynamic analysis of the planetary gearbox in a wind turbine," *Shock and Vibration*, vol. 2016, Article ID 9742673, 2016.

[13] A. Palermo, D. Mundo, R. Hadjit, and W. Desmet, "Multi-body element for spur and helical gear meshing based on detailed three-dimensional contact calculations," *Mechanism and Machine Theory*, vol. 62, pp. 13–30, 2013.

[14] A. Andersson and L. Vedmar, "A dynamic model to determine vibrations in involute helical gears," *Journal of Sound and Vibration*, vol. 260, no. 2, pp. 195–212, 2003.

[15] A. Fernandez Del Rincon, F. Viadero, M. Iglesias, P. García, A. De-Juan, and R. Sancibrian, "A model for the study of meshing stiffness in spur gear transmissions," *Mechanism and Machine Theory*, vol. 61, pp. 30–58, 2013.

[16] B. Guilbert, P. Velex, D. Dureisseix, and P. Cutuli, "A Mortar-Based Mesh Interface for Hybrid Finite-Element/Lumped-Parameter Gear Dynamic Models - Applications to Thin-Rimmed Geared Systems," *Journal of Mechanical Design*, vol. 138, no. 12, Article ID 123301, 2016.

[17] Y. Ren, S. Chang, G. Liu, L. Wu, and T. C. Lim, "Impedance synthesis based vibration analysis of geared transmission system," *Shock and Vibration*, vol. 2017, Article ID 4846532, 14 pages, 2017.

[18] J. D. Smith, *Gear Noise and Vibration*, Cambridge, 2003.